International Journal of Mechanical, Industrial and Aerospace Sciences
ISSN: 2517-9950
Vol:12, No:10, 2018

Estimation of the External Force for a Co-Manipulation Task Using the Drive Chain Robot

Sylvain Devie, Pierre-Philippe Robet, Yannick Aoustin, Maxime Gautier

***Abstract*—The aim of this paper is to show that the observation of the external effort and the sensor-less control of a system is limited by the mechanical system. First, the model of a one-joint robot with a prismatic joint is presented. Based on this model, two different procedures were performed in order to identify the mechanical parameters of the system and observe the external effort applied on it. Experiments have proven that the accuracy of the force observer, based on the DC motor current, is limited by the mechanics of the robot. The sensor-less control will be limited by the accuracy in estimation of the mechanical parameters and by the maximum static friction force, that is the minimum force which can be observed in this case. The consequence of this limitation is that industrial robots without specific design are not well adapted to perform sensor-less precision tasks. Finally, an efficient control law is presented for high effort applications.

***Keywords*—Control, Identification, Robot, Co-manipulation, Sensor-less.

I. Introduction

FORCE control is an important part of the mechatronic control [1]. This type of control system is currently made by using force sensors in order to measure the external effort. However, in particular cases, this solution cannot be applied and a sensor-less solution by using motor currents has to be chosen. For example, in [2], the electrical current measurement is used to estimate the feed cutting force for a manufacturing operation. In [3], the current of the DC motors of a legged walking robot was used to estimate the ground reaction force based on the dynamic equation in the joint space for each joint. The inner friction were identified by using a neural network to improve the identification. Recently, Kambara *et al.* have proposed, in [4], an innovative disturbance force observer based on the model of their minor current loop. Then this observer is used to carry out acceleration-based control for tele-operation tasks without external force sensor and have proven its efficiency by comparing it to more classical observation-based controls.

In the case of force control, and more specifically in case of co-manipulation tasks, the external perturbations are mostly due to the mechanical part of the system. These perturbations have a direct effect on the observation of the effort and have to be identified or mechanically compensated. For example, the Haption master arm [5] has been designed in order to be mechanically transparent. This means that all the mechanical losses are compensated and the effort given by the actuator is exactly equal to the effort applied on the environment by the end-effector. With this design, sensor-less force control can be performed for surgical tasks. In the case of industrial robots, the power from the actuator is shared between the useful work, dynamic effects like inertia or the Coriolis effect, and perturbation effects like friction. In this spirit, in [6] the authors proposed a friction observer in order to control industrial robots by using an innovative estimation of the friction perturbation.

In the case of the co-manipulation control, the perturbation are be divided into two categories: the effort from the operator and the friction perturbation. The effort from the operator is one of the inputs of the control law. In the classical application, we desire the velocity of the robot to be proportional to this effort. The friction perturbation consists of mechanical losses in the transmission which consumes energy between the actuator and the end-effector. The identification of these perturbation presents some difficulties. For example, the *break-away*, between the state of rest and motion is difficult to define, and several empirical models have been proposed [7]-[9]. Another difficulty is the non-repeatability of the friction identification, which makes the friction compensation difficult [10], [11]. This difficulty can be minimised with on-line correction of the friction estimation. For example, in [12] the friction estimation is corrected on-line in order to carry out impedance control.

More globally, the mechanical parameters of an industrial robot are estimated with a general identification method, based on the inverse dynamic model (IDM) and the least squares (LS) method. This method has been successfully applied to identify the inertial and friction parameters of many prototypes and industrial robots [13], [14]. The identification consists of moving a robot without a load (or external force) or with a constant given payload [15], by following a specific trajectory [16]. More complicated models can also be solved in order to consider the flexibility of the system [17].

The aim of this paper is to illustrate the limit for the force observation for an industrial robot in the case of a co-manipulation task. This task is similar to the tele-operation task presented in [4]. The difference is that in the case of co-manipulation a single robot is considered and the force applied at its end-effector by the operator is the reference effort that the robot has to follow, while two robots are considered in the case of tele-operation: the force applied on one robot is the reference for the force applied by the other one. For the experimental part, a one-link robot with a prismatic joint is presented and is assumed to be rigid. This robot testbed has already been used to test several identification processes over the last few years [18], [17] and is

Sylvain Devie, Pierre-Philippe Robet, Yannick Aoustin and Maxime Gautier are with the LS2N (Digital Sciences Laboratory of Nantes), France (e-mail: Sylvain.Devie@univ-nantes.fr, Pierre-philippe.Robet@univ-nantes.fr, Yannick.Aoustin@univ-nantes.fr, Maxime.Gautier@univ-nantes.fr).

a good tool to perform this kind of study, as recently shown in [19]. There, an acceleration-based impedance control is used in a tele-operation scenario for fast environmental stiffness estimations with a time delay. Or in [20] where the bilateral control is improved by considering a non-linear model for the perturbation observer.

From the work of Onishi [1] a force observer is first implemented for our robot. An identification of its parameters was a priori made. The aim of this force observer will be to check if it is possible to perform a precise task with a low force observer. After that, an impedance based control law based on Hogan's [21], [22] work is implemented. This control law allows us to successfully perform co-manipulation tasks with large external forces. In [23], an equivalence was shown between this control law and the one already used in the harware used in this paper [24], [25].

This paper is outlined as follows. Section II focuses on the model of the robot and presents its Newton-Euler equation in order to define a linear form of the Inverse Dynamic Model. Section III uses this model to perform the identification of the mechanical parameters of the robot and the observation of the effort of the operator while performing a co-manipulation task. Section IV proposes an efficient sensor-less control law for high forces and Section V offers our conclusion and perspectives.

II. Modeling of a Rigid Industrial Robot

A. Experimental Set-Up

The EMPS is a high-precision linear Electro-Mechanical Positioning System, presented in Fig. 1. It is a standard configuration of a drive system for the prismatic joint of robots. It is actuated by a Maxon DC motor which drives a carriage by a ball screw. The carriage moves a force sensor and a gripper in translation. The motor rotor and the ball screw are connected by a flexible coupling. Two incremental encoders are presented on the robot. The first one measures the motor position q_m (rad) while the second one measures the position of the ball screw q_1 (rad).

For the applications considered in this paper, the robot is assumed to be rigid in the frequency range of the system harmonics. This means that the encoder measurements are equal and $q_m = q_1$. In the following, we will consider only the displacement of the carriage $q = q_m/r$ (m), where r is the pitch of the ball-screw (rad/m).

An inner current loop is physically integrated at the input of the DC motor and allows it to control the motor without using the current sensor. This helps the hardware of the system becomes simpler. This current regulation cannot be easily modified by the operator and has a frequency ω_I 20 times greater than the velocity loop. In the following, the current loop will be assimilated into a simple gain.

In the following, all the variables on the load side will be given in SI units. The force applied by the motor on the carriage is linearly proportional to the motor torque with a factor of the reduction ratio of the ball screw r. This torque is linearly proportional to the current sent to the motor I_m (A), with a factor of the torque constant k_t (N/A). A current amplifier is present on the input of the current loop v_I (V), with $I_m = G_i v_I$.

In the following, we will consider:

$$\tau_m = G_i \ r \ k_t \ v_I = G_\tau v_I \tag{1}$$

The parameter G_τ (N/V) will be considered to be known and independent of the experimental conditions.

B. Inverse Dynamic Model of the Robot

The mechanical system, presented in Fig. 2 has one prismatic degree of freedom q (m). It is affected by the actions of the motor τ_m (N) and of the environment τ_e (N). In the considered case, the body of the robot is not affected by gravitational force.

The Inverse Dynamic Model (IDM) calculates the motor force as a function of the joint position and its derivatives. Newton-Euler equations give the following IDM [26]:

$$\tau_m + \tau_e = M\ddot{q} + F_v\dot{q} + F_c \mathrm{sign}(\dot{q}) \tag{2}$$

Here:

- $\dot{q}$ (m/s) and $\ddot{q}$ (m/s^2) are respectively the carriage velocity and acceleration,
- τ_m (N) is the drive force from the motor,
- M (kg) is the total load side equivalent mass, including the inertia of all rotating elements in the drive chain and the mass of all the translating elements,
- τ_e (N) is the external force, applied by the environment,
- F_v $(N/m/s)$ is the viscous damping coefficient,
- F_c (N) is the Coulomb friction force,
- $\mathrm{sign}(u)$ denotes the sign function.

The friction considered here, as shown in Fig. 3, is a classical model that takes into account only the kinetic (Coulomb) friction and viscous damping:

$$F_{fc}(\dot{q}) = F_v\dot{q} + F_c \mathrm{sign}(\dot{q}) \tag{3}$$

However, this model does not take into account the static friction: in the static case, a break-away force F_s (N) is needed to overcome the static friction and move the robot, with $F_s > F_c$. This *break-away* is very difficult to model efficiently, the most efficient empirical model to approximate it is the Stribeck model, taking into account the non-linearity due to adherence at the null velocity:

$$F_{fs} = F_v\dot{q} + F_c \mathrm{sign}(\dot{q}) + (F_s - F_c)\mathrm{e}^{-|\dot{q}/\dot{q}_s|^{\delta_s}} \mathrm{sign}(\dot{q}) \tag{4}$$

where $\dot{q}_s$ (m/s) is the Stribeck velocity constant and δ_s is a coefficient between 1 and 2. The shape of this model is also presented in Fig. 3. The classical model restricts us to experiments in areas far from the non-linear area, away from null velocities.

Another model problem would be the unsymmetrical behaviour of friction [18]. In order to deal with this, a two quadrant model will be considered for the Coulomb and viscous friction, depending on the sign of the speed. This implies the following:

- F_c^+, F_v^+ and $\dot{q}^+$ will respectively be used for F_c, F_v and $\dot{q}$ when $\dot{q} > 0$

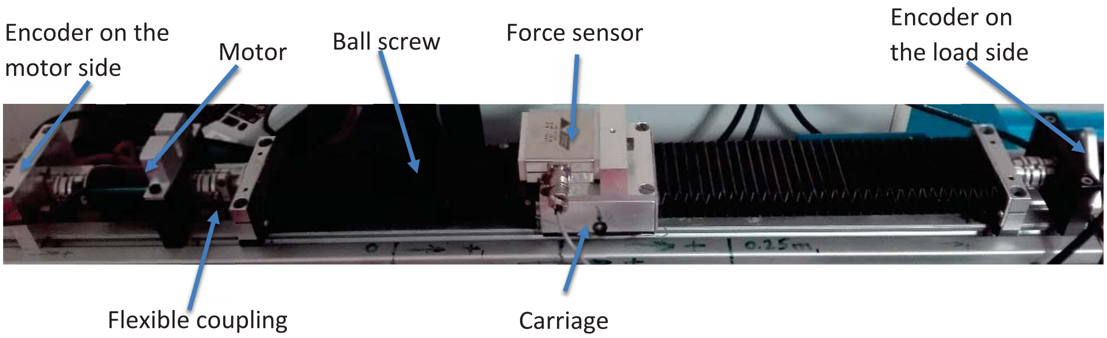

Fig. 1 Components of the EMPS robot

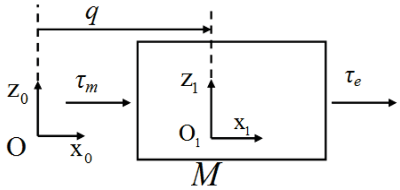

Fig. 2 Components of the EMPS robot

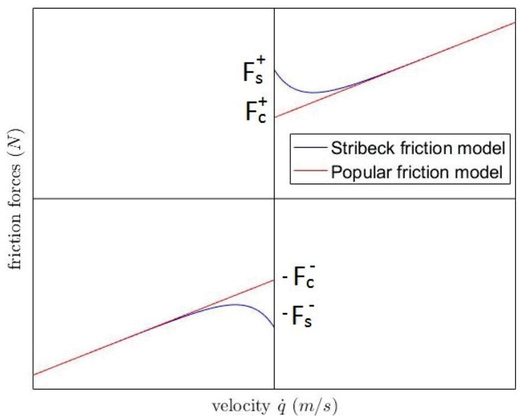

Fig. 3 Shape of the classical friction model in red, and the Stribeck friction model in blue, function of the velocity $\dot{q}$

- F_c^-, F_v^- and $\dot{q}^-$ will respectively be used for F_c, F_v and $\dot{q}$ when $\dot{q} < 0$

Equation (2) can be re-written as function of the model parameters, gathered in vector $\mathbf{X}$.

$$\tau_m + \tau_e = \mathbf{W}\mathbf{X} \tag{5}$$

Here:

- $\mathbf{X} = \begin{bmatrix} M & F_v^+ & F_v^- & F_c^+ & F_c^- \end{bmatrix}^\top$ is a 5×1 vector
- $\mathbf{W} = \begin{bmatrix} \ddot{q} & \dot{q}^+ & \dot{q}^- & \text{sign}(\dot{q}^+) & \text{sign}(\dot{q}^-) \end{bmatrix}$ is a 1×5 matrix.

This equation will be used in the following in order to identify the parameters in $\mathbf{X}$.

C. Control Design

In a previous study [24], a simple control law was studied for the force control using an integral proportional (IP) correction for the velocity loop and a proportional (P) correction for the force loop. Then this control law was adapted in order to perform the co-manipulation task.

In a co-manipulation case, the environmental impedance depends on the impedance of the environment and of the operator's hand. This environmental impedance is supposed to be unknown. In this case, a classical control system is illustrated in Fig. 4. Here, an inner velocity loop is used to control the performance of the system while an outer force loop is used to control its transparency. Increasing the gain k_{e1}, we increase the transparency. However, a too high gain can lead to instability. The aim is to get a simple co-manipulation controller with $\tau_e = 0$ when the robot is not moving ($\dot{q}_1 = \dot{q}_2 = 0$). It leads us to choose the force reference $\tau_{ref} = 0$ which is the offset of the force the operator has to apply on the system.

Thanks to this reference, the system allows a linear relationship between the external force τ_e and the velocity reference $v_{\dot{q}}$. If the external perturbation has a low frequency, the relation $\tau_e = k_c \dot{q}_1$ can be used in order to calculate the correction gains of the closed loops.

In order to calculate the correction and the performance of the system, we consider that the frequency range ($< 20\ rad/s$) of the exogenous disturbance τ_e is small compared to the bandwidth of the velocity loop ($100\ rad/s$), in order to provide a linear relation between the velocity and the external force: $\tau_e = k_c \dot{q}_1$ with $k_c = 1/k_{e1}$. However, in the case of low external forces, the external force can be neglected for the calculation of the velocity loop correction. According to Fig. 4 and considering this last assumption, for co-manipulation applications the open loop transfer function of the velocity loop is given by the equation:

$$T_{vo}(s) = \frac{\dot{q}_1(s)}{v_{\dot{q}}(s) - \dot{q}_1(s)} = \frac{k_{v1} G_\tau}{t_v s} \frac{1}{M_1 s + F_{v1} + k_{v1} G_\tau} \tag{6}$$

Imposing the phase margin ϕ_v at a frequency ω_v leads to $T_{vo}(j\omega_v) = 1 e^{j(-\pi + \phi_v)}$ and gives the values of k_{v1} and t_v [?].

$$k_{v1} = \frac{M_1 \omega_v \tan(\phi_v) - F_{v1}}{G_\tau}, \; t_v = \frac{k_{v1} G_\tau}{M_1 \omega_v^2} \cos(\phi_v) \tag{7}$$

The closed loop transfer function for the velocity loop is:

$$T_{vc}(s) = \frac{\dot{q}_1(s)}{v_{\dot{q}}(s)} = \frac{1}{1 + (t_v + \frac{F_{v1}}{K_v})s + \frac{M_1}{K_v} s^2} \tag{8}$$

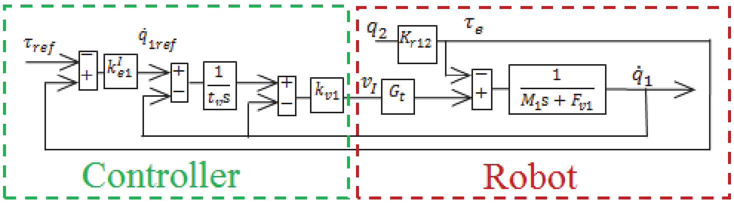

Fig. 4 Cascaded closed loop of speed and force in the case of co-manipulation

with $K_v = k_{v1} G_\tau / t_v$. Let us write this transfer function in the canonical form:

$$T_{vc}(\mathrm{s}) = \frac{1}{1 + \frac{2z_v}{\omega_{0v}}\mathrm{s} + \frac{\mathrm{s}^2}{\omega_{0v}^2}} \quad (9)$$

with $\omega_{0v} = \sqrt{K_v/M_1}$ and $z_v = (t_v + \frac{F_{v1}}{K_v})\frac{\omega_{0v}}{2}$.

The outer open force loop has the following equation:

$$T_{eo}(\mathrm{s}) = \frac{\tau_e}{\tau_{ref} + \tau_e} = \frac{k_{e1} k_c}{1 + \frac{2z_v}{\omega_{0v}}\mathrm{s} + \frac{\mathrm{s}^2}{\omega_{0v}^2}} \quad (10)$$

According to the definition of k_c, which is equivalent to a viscous friction coefficient, the equation can be written in the following form:

$$T_{eo}(\mathrm{s}) = \frac{1}{1 + \frac{2z_v}{\omega_{0v}}\mathrm{s} + \frac{\mathrm{s}^2}{\omega_{0v}^2}} \quad (11)$$

Here, the coefficient k_c is chosen to provide good transparency.

III. Reaction Force Observer for Small External Forces

A rigorous observation of the reaction force needs a perfect estimation of the electro-mechanical parameters of the system. Hence, the observation of the reaction force needs two steps: the identification of the system parameters, and the estimation of the reaction force from the parameters. In the considered case, the electrical parameters are perfectly known and used to control the inner velocity loop, however the mechanical parameters have to be identified.

A. Identification of the Parameters

Considering an acquisition free of reaction force, with a position control of the robot allowing it to follow a specific trajectory, (5) becomes:

$$\tau_{\mathbf{m1}} = \mathbf{W_1 X_1} \quad (12)$$

Where $\tau_{\mathbf{m1}}$ is a $n \times 1$ matrix of motor forces, $\mathbf{X_1}$ is a $p \times 1$ matrix of mechanical parameters and $\mathbf{W_1}$ is $n \times p$ matrix of velocity and acceleration signals calculated numerically from the measured positions. Here $p = 5$ is the number of independent parameters and n is the number of samples. In this section, the subscript $_1$ is used to describe data from the first set of experiments related to identification.

According to this model, for a robot following a dynamic trajectory [16], the matrix $\widehat{\mathbf{X}}_\mathbf{1}$ can be estimated with the least squares method, for example by using the Matlab function: $\widehat{\mathbf{X}}_\mathbf{1} = \mathbf{W_1} \setminus \tau_{\mathbf{m1}}$

Standard deviations are estimated using classical and simple results from statistics, considering the matrix $\mathbf{W}_1$ to be a deterministic one, and ρ to be a zero mean additive independent noise, with standard deviation $\sigma_{\rho\rho}$ such that:

$$\mathbf{C}_{\rho\rho} = \mathrm{E}(\rho\rho^\top) = \sigma_\rho^2 \mathbf{I_N} \quad (13)$$

where E is the expectation operator and $\mathbf{I}_n$ is the $(n \times n)$ identity matrix. An unbiased estimation of σ_ρ is used and given by the expression:

$$\widehat{\sigma}_\rho^2 = \frac{\| \tau_{\mathbf{m1}} - \mathbf{W_1}\widehat{\mathbf{X}}_\mathbf{1} \|^2}{n-p} \quad (14)$$

The variance-covariance matrix of the estimation error and standard deviations can be calculated by:

$$\mathbf{C}_{\widehat{\mathbf{X}}_1\widehat{\mathbf{X}}_1} = \mathrm{E}[(\mathbf{X_1} - \widehat{\mathbf{X}}_\mathbf{1})(\mathbf{X_1} - \widehat{\mathbf{X}}_\mathbf{1})^\top] = \sigma_\rho{}^2(\mathbf{W_1}\mathbf{W_1}^\top)^{-1} \quad (15)$$

The relative standard deviation is given by the expression:

$$\%\sigma_{\widehat{\mathbf{X}}_1}(i) = 100 \left| \frac{\widehat{\sigma}_{\widehat{\mathbf{X}}_1}(i)}{\widehat{\mathbf{X}}_\mathbf{1}(i)} \right| \quad (16)$$

where $\sigma_{\widehat{\mathbf{X}}_1}{}^2(i) = \mathbf{C}_{\widehat{\mathbf{X}}_1\widehat{\mathbf{X}}_1}(i,i)$ is the i^{th} diagonal coefficient of $\mathbf{C}_{\widehat{\mathbf{X}}_1\widehat{\mathbf{X}}_1}$.

Because of the perturbations due to the noise and the modeling errors, the actual force $\tau_{\mathbf{m1}}$ differs from the estimated one $\widehat{\tau}_{\mathbf{m1}}$ by an error $\mathbf{e_1}$, such that:

$$\tau_{\mathbf{m1}} = \widehat{\tau}_{\mathbf{m1}} + \mathbf{e_1} = \mathbf{W_1}\widehat{\mathbf{X}}_\mathbf{1} + \mathbf{e_1} \quad (17)$$

Calculating the least squares solution (17) from the data in $\mathbf{W_1}$ and $\tau_{\mathbf{m1}}$ can lead to a bias if $\mathbf{W_1}$ is correlated to $\mathbf{e_1}$. Hence, it is essential to filter the data in $\tau_{\mathbf{m1}}$ and $\mathbf{W_1}$ before computing $\mathbf{W_1} \setminus \tau_{\mathbf{m1}}$.

Velocities are directly estimated by a backward derivative of the position, and the acceleration is estimated by a central derivative of the filtered velocity. All the variables were corrected with the *medfilt1* and *decimate* functions of Matlab ®The measured and filtered values of the effort from the motor τ_{m1}, the velocity $\dot{q}$ and the acceleration $\ddot{q}$ are presented in Fig. 5.

The velocity reference trajectory is a mixture of trapezoidal segments and constant velocity segments. Specific shapes of the trajectory highlight specific dynamic parameters. A linear variation of the velocity highlights the inertial parameters while a constant velocity highlights the viscous friction parameters. The reference trajectory is optimized in order to have a linear variation of velocity half the time, and a constant velocity in the other half of the time, in order to excite all the parameters in order to identify each of them with a good accuracy.

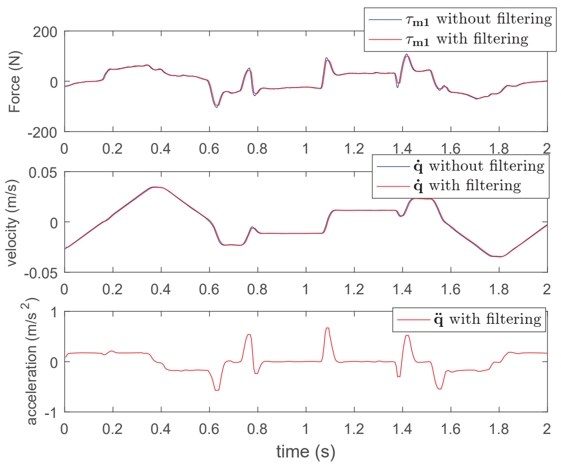

Fig. 5 Measured values (blue) and filtered values (red) of the effort from the motor (top), the velocity (middle) and the acceleration (bottom)

Ten experiments were performed in order to identify the parameters of the robots. Fig. 6 shows the evolution of the motor effort $\tau_{\mathbf{m1}}$ calculated thanks to the motor current measurement and its estimated values without taking the error into account $\mathbf{W_1X_1}$.

The identified values for the experiment shown in Fig. 6 are given in Table I.

TABLE I
IDENTIFIED VALUES

parameters	$\widehat{\mathbf{X}}_\mathbf{1}$	$2\widehat{\sigma}_{\widehat{\mathbf{X}}_\mathbf{1}}$	$\%\sigma_{\widehat{\mathbf{X}}_\mathbf{1}}$
M_1 (kg)	115.7315	0.5765	0.4981
F_{v1}^+ (N/m/s)	474.9727	17.5686	3.6989
F_{v1}^- (N/m/s)	563.8568	19.3088	3.4244
F_{c1}^+ (N)	17.3811	0.3259	1.8750
F_{c1}^- (N)	11.5846	0.3363	2.9030

It is important to remark that for the experiment presented in Fig. 6, the estimated Coulomb frictions is $F_{c1}^+ = 17\ N$. Another static experiment allowed us to estimate the static friction as $F_s^+ = 17\ N$. This means that the classical model used for the observation is well adapted for a ball screw system. That also means that, in the case of sensor-less control, the operator has to apply a break-away force $\tau_e = 17\ N$ on a static robot in order to allow the controller to detect its action.

The root mean square (RMS) error between the motor force $\tau_{\mathbf{m1}}$ and $\mathbf{W_1X_1}$ is $RMS_1 = \sqrt{\text{mean}(\mathbf{e_1}^2)} = 3.6\ N$. The errors from the other experiments varies between $3.6\ N$ to $5.3\ N$. This identification will be used for the observation in the next step. This means that the observer cannot be more accurate than $3.6\ N$ in the best case.

In the following, $\widehat{\overline{\mathbf{X}}}_\mathbf{1}$ represents the mean value of the mechanical parameters of $\widehat{\mathbf{X}}_\mathbf{1}$ and which were calculated with the ten experiments.

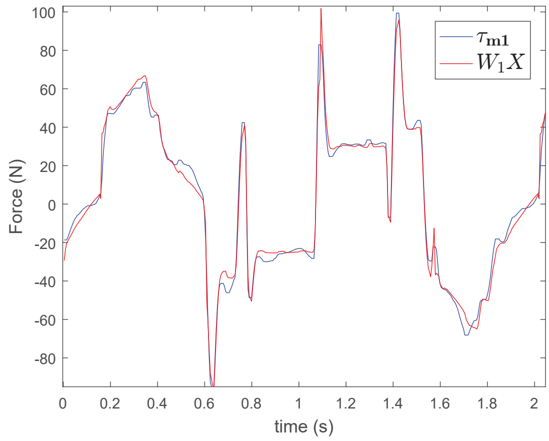

Fig. 6 Force from the motor $\tau_{\mathbf{m1}}$ in blue and $\mathbf{W_1X_1}$ in red

B. Observation of the Reaction Force

Once the model is known, the goal is to observe the reaction of the external forces. The co-manipulation control law presented in the previous section is considered. The aim of this operation is to control a robot with a transparent behaviour. This means that the operator should hold a gripper at the end-effector of the robot and move it without feeling the dynamics of the robot. This can be achieved thanks to high values of the gains of the outer force loop. However, we want to estimate the force applied by the operator on the robot. This interaction effort can be improved by reducing the transparency of the control law. The first step to perform a sensor-less task: if the estimation of the force τ_e is not efficient enough, the control of the force τ_m is impossible with any control law.

The control law presented in Section II-C is used with the FN3280 sensor from Hoskin. The data collected thanks to this sensor is used to control the robot and will be compared to the estimated effort $\widehat{\tau}_{\mathbf{e1}}$ from the observer.

Here, the aim is to observe the external force τ_{e1}. If the control system is transparent, the operator does not feel the force from the robot, and its action is compensated by the control system. In this case, the observation of the motor torque does not allow us to estimate this force. To avoid this issue, the gain k_{e1} is chosen to have a poor transparency of the system. The effort measured by the force sensor will be considered equal to the real effort from the operator, as the sensing error is insignificant compared to the identification error.

This effort is estimated with the help of (5), as follows:

$$\tau_{\mathbf{e2}} = \tau_{\mathbf{m2}} - \mathbf{W_2X_2} \tag{18}$$

In this section, the subscript $_2$ is used to describe data from the second set of experiments related to the observer. The vector $\widehat{\overline{\mathbf{X}}}_\mathbf{1}$ from the mechanical parameters identified in the previous experiments will be considered instead of the vector $\mathbf{X_2}$.

Ten experiments were performed in a co-manipulation scenario, they are illustrated by Fig. 7. During these

Fig. 7 Co-manipulation experiments, the operator apply a specific force on the force sensor of the robot presented into Fig. 1

experiments, a co-manipulation task was carried out, considering a non-null reference force in order to ensure an effort at any time. For each of these experiments, the force applied by the operator on the system was estimated by:

$$\widehat{\tau}_{\mathbf{e2}} = \mathbf{W_2}\widehat{\widehat{\mathbf{X}}}_\mathbf{1} - \tau_{\mathbf{m2}} \tag{19}$$

With $\tau_{\mathbf{m2}}$ calculated with the help of (1). Again, because of the perturbations due to the noise, the modeling errors, and the identification errors, the actual force $\tau_{\mathbf{e2}}$ applied by the operator differs from $\widehat{\tau}_{\mathbf{e2}}$ by an error $\mathbf{e_2}$ depending on $\mathbf{e_1}$, such that:

$$\tau_{\mathbf{e2}} = \widehat{\tau}_{\mathbf{e2}} + \mathbf{e_2} \tag{20}$$

Two main cases of the calculation of $\tau_{\mathbf{m2}}$ can be considered: the on-line calculation and the **off-line** calculation. The on-line calculation is done during the experiment, with a simple first-order low pass filter on the measured velocity and current in order to obtain a real time estimation of the force, which can be used to perform a sensor-less co-manipulation operation. The off-line calculation is done after the experiment and allows better filtering of the data.

Considering the off-line calculation, the force applied by the operator is calculated by (19). The force measured by the sensor τ_{e2} and the estimated force $\widehat{\tau}_{e2}$ are presented on Fig. 8.

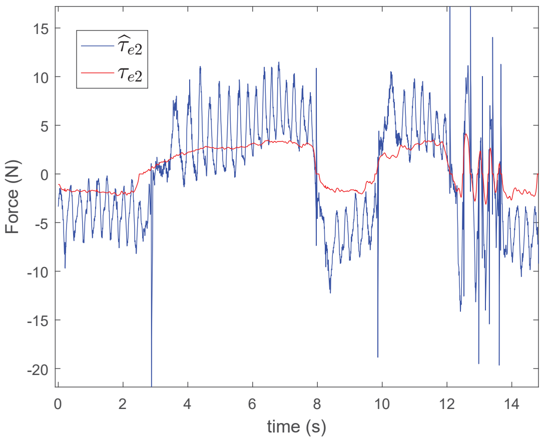

Fig. 8 Force measured by the sensor τ_{e2} in red and estimated force $\widehat{\tau}_{e2}$ in blue

According to this figure, for a small force from the operator, the noise from the observer is bigger than the actual effort.

For the ten experiments, the RMS error of the observation $RMS_2 = \sqrt{\text{mean}(\mathbf{e_2}^2)}$ varies from 3.9 N to 5.4 N. This result proves that the force observation with a simple 2 quadrant mechanical model is not well adapted for precision tasks.

However, the proposed model uses a cross validation of the observer - the observed effort is calculated thanks to the data identified with another experiment. This means that the error $\mathbf{e_2}$ from the second experiment accumulates upon the error $\mathbf{e_1}$ from the first experiment. This problem is cumulated with another one due to the characteristics of the stiffness: it is non-homogeneous on the full workspace of the robot and depends on several parameters, like the lubrication or the temperature. In our case, the used workspace was sufficiently small and the time between the two steps was sufficiently small to consider the estimation to be correct. However, in the case of industrial robots, the parameters identified in the first step could differ from the parameters which should be used in the second step.

Another approach to limit these errors is to carry out the two steps on the same set of data off-line.

C. Direct Validation Observation

Let us now consider only the co-manipulation experiment from the previous section. The efforts applied by the operator were specifically chosen in order to present particular behaviours like ramps and floors allowing the identification of the system. Here, the aim is not to propose a strategy for sensor-less control, but to use an identification and observation protocol based on force measurement to check the efficiency of the previous calculations.

Let us now consider (5):

$$\mathbf{Y} = \tau_\mathbf{m} + \tau_\mathbf{e} = \mathbf{WX} \tag{21}$$

Here, $\tau_{\mathbf{m1}}$ is calculated thanks to the current measurement and (1), $\tau_{\mathbf{e1}}$ is given by the force sensor and $\mathbf{W}$ is calculated off-line thanks to the motor encoder and time derivative computations.

According to the previous section, the dynamic parameters in $\mathbf{X}$ can be estimated by $\widehat{\mathbf{X}}$ with the help of a least squares method in order to approximate $\mathbf{Y}$, with:

$$\mathbf{Y} = \mathbf{W}\widehat{\mathbf{X}} + \mathbf{e_i} \tag{22}$$

where $\mathbf{e_i}$ is the vector of the identification error for the experiment, due to measurement noise and modelling errors.

The effort from the operator can be estimated similar to the previous section, by:

$$\widehat{\tau}_\mathbf{e} = \mathbf{W}\widehat{\mathbf{X}} - \tau_\mathbf{m} \tag{23}$$

The evolution of this effort is presented in Fig. 9, for the same experiment as in Fig. 8.

The identified values for the experiment shown in Fig. 6 are given in Table II

TABLE II
IDENTIFIED VALUES

parameters	$\widehat{\mathbf{X}}_\mathbf{1}$	$2\widehat{\sigma}_{\widehat{\mathbf{X}}_\mathbf{1}}$	$\%\sigma_{\widehat{\mathbf{X}}_\mathbf{1}}$
M_1 (kg)	109	1.24	1.13
F_{v1}^+ (N/m/s)	707	27.5	3.89
F_{v1}^-(N/m/s)	998	26.4	2.65
F_{c1}^+ (N)	18.9	0.21	1.15
F_{c1}^- (N)	9.8	0.21	2.22

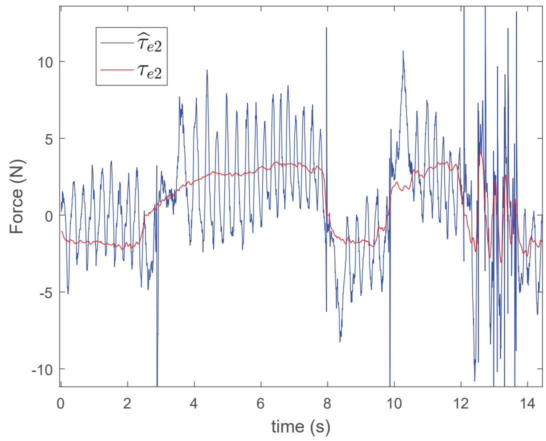

Fig. 9 Force measured by the sensor τ_e in red and estimated force $\widehat{\tau}_e$ in blue

The RMS error between the observed force and the actual effort from the operator is 2.8 N. For the ten experiments, this error varies from 2.7 N to 3.4 N, which is of the same order of magnitude as the value of the forces applied by the operator, but better than the observations of the previous section.

These results are mostly due to the fact that most of the power from the motor is used to compensate for the dynamics of the robot, and not to assist the operator. This means, in (23), τ_m is approximately equal to $W\widehat{X}$. This assumption is illustrated in Fig. 10.

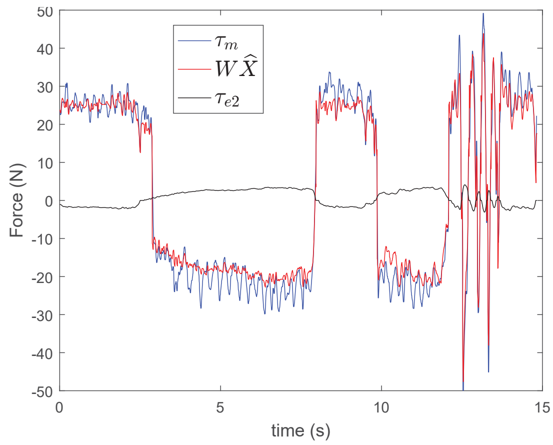

Fig. 10 Force applied by the motor τ_m in blue, and estimated force $W\widehat{X}$ in red and effort from the operator τ_e in black

According to this figure, the motor forces and the forces due to the mechanical losses have a maximum value of 30 N, while the maximum value of the effort from the operator is equal to 5 N, which is the range of the sensing device. In this particular case, the effort applied by the operator has the same order of magnitude as the precision of the observation.

Several techniques can be proposed to reduce this problem. The most common technique is to design a specific robot with a mechanical compensation of the mechanical losses. In this case, the force needed to move the robot $W\widehat{X}$ would be far smaller, and the force from the motor would be equal to the force from the operator. Another way to reduce the problem would be to perform large force operations instead of precision operations in order to have a force τ_e higher than the precision of the observation. In this configuration, we can assume a good reconstruction of the force τ_e. In any case, it appears that a sensor-less force control is not possible in the case of small forces for co-manipulation applications with industrial robots. However, the next section will present an efficient control law allowing for these kinds of applications for large external forces.

IV. Sensor-Less Co-Manipulation Control for Large External Forces

The aim of this section is to present an efficient control law in order to carry out a sensor-less co-manipulation task with an industrial robot, for large external forces based on on-line estimation of the operator force. Unfortunately, the available hardware does not allow the measurement of large forces on the system, so it is not possible to compare the evolution of the external force and the movement of the system. Simulation results are presented and external videos have proven the efficiency of the control law on a real device.

In this section, in order to simplify the expression, we consider only a one quadrant model: we consider the friction coefficients to be symmetric and not dependant on the sign of the velocity.

A. Control Design

The control law used in this section is different from the one used in the Section II-C. The previous control law is more efficient for systems controlled with a force sensor. In this case, the external force usually varies at a low frequency, which allows the use of an external force loop giving the reference of the inner velocity loop as shown in Fig. 4. However, in the case of a sensor-less control law, the estimated effort depends on the velocity for the estimation of the friction and the electric current for the estimation of the motor force. In our specific hardware, an inner electrical current loop is implemented and has a bandwidth 20 times higher than that of the bandwidth of the velocity loop.

In the case of large external forces, it is possible to apply an impedance control law on the system and control the motor torque to achieve the desired dynamic performance. Fig. 11 describes the implementation of the impedance control law and its model. The impedance control is used to control the motor torque according to the current velocity $\dot{q}$ (m/s), the motor electric current I_m (A), and a reference position q_0 (m), as presented in Fig. 11a. The aim is to control the apparent impedance, described by Fig. 11b with M_a, B, and K, around the position q_0.

According to (2), the mechanical equation used to design the control law is:

$$\tau_m + \tau_e = \hat{M}\ddot{q} + \hat{F}_v\dot{q} + \hat{F}_c\text{sign}(\dot{q}) \quad (24)$$

with $\hat{M}$, $\hat{F}_v$ and $\hat{F}_c$ identified in the previous section.

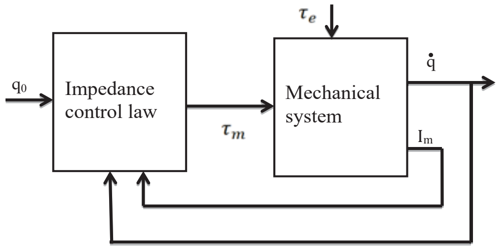

(a) Implementation of the impedance control

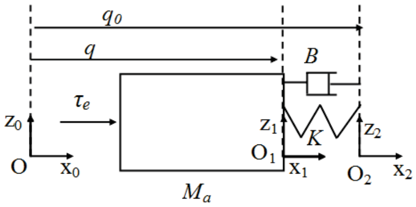

(b) Description of the desired impedance

Fig. 11 Definition of the impedance control law

According to Fig. 11b, the desired mechanical equation is the following:

$$\tau_e = M_a\ddot{q} + B(\dot{q} - \dot{q}_0) + K(q - q_0) \tag{25}$$

This equation gives:

$$\ddot{q} = \frac{1}{M_a}(\tau_e - B(\dot{q} - \dot{q}_0) - K(q - q_0)) \tag{26}$$

According to (24) and (26), we get:

$$\begin{aligned} \tau_m &= (\frac{\hat{M}}{M_a} - 1)\tau_e + (\hat{F}_v - \frac{\hat{M}}{M_a}B)(\dot{q} - \dot{q}_0) \\ &+ \hat{F}_c\text{sign}(\dot{q}) - \frac{\hat{M}}{M_a}K(q - q_0) \end{aligned} \tag{27}$$

Equation (27) is a classical impedance control law with a prediction term correcting the friction effects. In the following, in order to perform a co-manipulation task, we consider the following simplifications: $K = 0$ and $\dot{q}_0 = 0$. Thus, (27) becomes:

$$\tau_m = (\frac{\hat{M}}{M_a} - 1)\tau_e + (\hat{F}_v - \frac{\hat{M}}{M_a}B)\dot{q} + \hat{F}_c\text{sign}(\dot{q}) \tag{28}$$

Let us now define the following external force observer:

$$\hat{\tau}_e = \hat{M}\ddot{q} + \hat{F}_v\dot{q} + \hat{F}_c\text{sign}(\dot{q}) - G_{\tau i}I_m \tag{29}$$

where I_m (A) is the current in the current loop of the motor. For our model, we consider $\hat{\tau}_m = G_{\tau i}I_m$. With $G_{\tau i} = k_t r$, (28) and (29) give:

$$\begin{aligned} \tau_m &= (\frac{\hat{M}}{M_a} - 1)\hat{M}\ddot{q} + \frac{\hat{M}}{M_a}(F_v - B)\dot{q} + \frac{\hat{M}}{M_a}F_c\text{sign}(\dot{q}) \\ &- 2(\frac{\hat{M}}{M_a} - 1)G_{\tau i}I_m \end{aligned} \tag{30}$$

B. Simulation Result

Simulations were performed using the impedance control law (30). The parameters M_a and B are calculated from the parameters of the control law of Section II-C thanks to an equivalence criterion. The parameters $\hat{M}$, $\hat{F}_v$ and $\hat{F}_c$ are the ones identified in Section III-A, when $\dot{q} > 0$.

The simulation is performed considering an identification error of 2% between the parameters used in the control law and the parameters used in the mechanic model. This error simulates the uncertainty of the identification.

The evolution of external force applied on the robot, its velocity and its position are plotted in Fig. 12. According to this figure, the control law allows a stable evolution of the velocity, proportional to the external force.

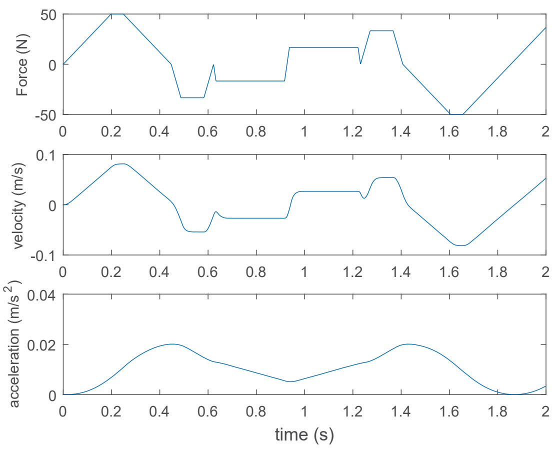

Fig. 12 Simulation of the external force $\tau_e(N)$, the velocity of the robot $\dot{q}(m/s)$ and its position $q(m)$ function of the time (s), for a co-manipulation application without force sensor

This result proves the efficiency of the force observer under these conditions. However, according to the hardware, the real conditions can be worse than the ones simulated. However, experiments were done with $M_a = 50\ kg$ and $B = 100\ N/(m/s)$. The result can be seen on the videos.

It appears that the operator has to apply an effort higher that in the case , where a force sensor is used. It is coherent with the results of the previous section.

V. Conclusion

The aim of this paper was to show the limits of force observation in the case of co-manipulation tasks with an industrial robot. Firstly, the model of the robot was defined, and presented in a linear form. This model was used to perform identification of the robot parameters and observation of the external effort based on the current in the DC motor. It appears that the identification of the mechanical parameters has a large variance. The consequence of this dispersion is a large error on the force observation. This error coupled with the effects of static friction makes it unsuitable for precise sensor-less applications.

Then, an efficient control law was presented in order to control the robot for sensor-less applications with large efforts.

Even if this application is less efficient that the one using a force sensor, due to noise and identification errors, it still gives acceptable results.

ACKNOWLEDGMENT

The project is co-funded by the European Union. Europe is now investing in Pays de la Loire with the European Regional Development Fund.

REFERENCES

[1] K. Ohnishi, M. Shibata, T. Murakami, and I. Paper, "Motion control for advanced mechatronics," *IEEE/ASME Trans. on Mechatronics*, vol. 1, no. 1, pp. 56–67, 1996.
[2] X. Li, A. Djordjevich, and P. K. Venuvinod, "Current-sensor-based feed cutting force intelligent estimation and tool wear condition monitoring," *IEEE Trans.on Industrial Electronics*, vol. 47, no. 3, pp. 697–702, 2000.
[3] C. Qi, F. Gao, Q. Sun, X. Chen, Y. Xu, and X. Zhao, "A foot force sensing approach for a legged walking robot using the motor current," *IEEE Conf. on Robotics and Biomimetics*, pp. 1078–1083, 2016.
[4] Y. Kambara and K. Ohnishi, "A design method of observers for bilateral control using dc brushed motor," *IEEE Industrial Electronics Society*, pp. 938–943, 2016.
[5] F. Gosselin, C. Bidard, and J. Brisset, "Design of a High Fidelity Haptic Device for Telesurgery," *IEEE Int. Conf. on Robotics and Automation*, no. April, pp. 205–210, 2005.
[6] C. Canudas de Wit, H. Olsson, K. Astrom, and P. Lischinsky, "A new model for control of systems with friction," *IEEE Trans. on Automatic Control*, vol. 40, no. 3, pp. 419–425, 1995.
[7] B. Armstrong-Helouvry, "Stick-slip arising from Stribeck friction," *IEEE Int. Conf. on Robotics and Automation*, vol. 2, pp. 1377–1382, 1990.
[8] D. P. Hess and A. Soom, "Friction at a Lubricated Line Contact Operating at Oscillating Sliding Velocities," *J. of Tribology*, vol. 112, no. 1, p. 147, 1990.
[9] L. C. Bo and D. Pavelescu, "The friction-speed relation and its influence on the critical velocity of stick-slip motion," *Wear*, vol. 82, pp. 277–289, 1982.
[10] J. W. Gilbart and G. C. Winston, "Adaptive compensation for an optical tracking telescope," *Automatica*, vol. 10, no. 2, pp. 125–131, 1974.
[11] C. D. Walrath, "Adaptive bearing friction compensation based on recent knowledge of dynamic friction," *Automatica*, vol. 20, no. 6, pp. 717–727, 1984.
[12] L. Roveda, G. Pallucca, N. Pedrocchi, F. Braghin, and L. Molinari Tosatti, "Iterative Learning Procedure with Reinforcement for High-Accuracy Force Tracking in Robotized Tasks," *IEEE Trans. on Industrial Informatics*, vol. 3203, no. c, pp. 1–10, 2017.
[13] P. Khosla and T. Kanade, "Parameter identification of robot dynamics," *IEEE Conf. on Decision and Control*, pp. 1754–1760, 1985.
[14] M. Gautier, "Numerical calculation of the base inertial parameters of robots," *J. of Robotic Systems*, vol. 8, no. 4, pp. 485–506, 1991.
[15] W. Khalil, M. Gautier, and P. Lemoine, "Identification of the payload inertial parameters of industrial manipulators," *IEEE Int. Conf. on Robotics and Automation*, pp. 4943 – 4948, 2007.
[16] M. Gautier and W. Khalil, "Exciting trajectories for the identification of base inertial parameters of robots," *IEEE Conf. on Decision and Control*, no. 4, pp. 2–7, 1991.
[17] M. Gautier, A. Jubien, A. Janot, and P. P. Robet, "Dynamic Identification of flexible joint manipulators with an efficient closed loop output error method based on motor torque output data," *IEEE Int. Conf. on Robotics and Automation*, pp. 2949–2955, 2013.
[18] P. Hamon, M. Gautier, P. Garrec, and A. Janot, "Dynamic Modeling and Identification of Joint Drive with Load-Dependent Friction Model," in *Int. Conf. on Advanced Intelligent Mechatronics*, 2010, pp. 902–907.
[19] D. Yashiro, "Fast Stiffness Estimation using Acceleration-based Impedance Control and its Application to Bilateral Control," in *IFAC World Congress*, 2017, pp. 12 565–12 570.
[20] K. Seki, S. Fujihara, and M. Iwasaki, "Improvement of Force Transmission Performance Considering Nonlinear Friction in Bilateral Control Systems," in *IFAC World Congress*, 2017, pp. 12 577–12 582.
[21] N. Hogan, "Impedance Control: An Approach to Manipulation," *J. of Dynamic Systems, Measurement, and Control*, vol. 107, no. March, pp. 304–313, 1985.
[22] ——, "Stable execution of contact tasks using impedance control," *IEEE Int. Conf. on Robotics and Automation*, vol. 4, pp. 1047–1054, 1987.
[23] S. Devie, P.-p. Robet, Y. Aoustin, and M. Gautier, "Impedance control using a cascaded loop force control ." *IEEE Robotics & Automation letter*, pp. 1–7, 2018.
[24] S. Devie, P. P. Robet, Y. Aoustin, M. Gautier, and A. Jubien, "Accurate force control and co-manipulation control using hybrid external command," *IFAC World Congress*, pp. 2271–2276, 2017.
[25] S. Devie, P.-p. Robet, Y. Aoustin, M. Gautier, and A. Jubien, "Optimized force and co-manipulation control using stiffness of force sensor with unknow environnement," *Robot Motion and Control, 2017. RoMoCo'17*, pp. 99–104, 2017.
[26] W. Khalil and E. Dombre, "Modeling, Identification and Control of Robots," *Applied Mechanics Reviews*, vol. 56, no. 3, p. 500, 2004.

Sylvain Devie received his Master's Degree in Advanced Robotics from the École Centrale de Nantes, and his Magister's Degree in Mechatronics from the École Normale Suprieure de Rennes in 2015. Since 2015, he has been a Ph.D. student in the Université de Nantes, working on the force control of robots in collaborative tasks.

Pierre-Philippe Robet received the Agrégation in electrical engineering from the Ecole Normale Suprieure, Cachan, France; the M.S. degree in satellite communication engineering from Surrey University, Guildford, United Kingdom; the Ph.D. degree from the Universit de Nantes et Ecole Centrale de Nantes, Nantes, France; in 1989, 1990, and 1996, respectively. Following receipt of the M.S. degree, he joined the International Maritime Satellite Organization to work in the eld of channel transmission modeling. Then, he was a teacher prior to begin his current research in automatic control and robotics at the University of Nantes and Ecole Centrale of Nantes. His current research topics include modeling, identication, control of electrical drives, and control of robots with force feedback.

Yannick Aoustin is Professor at University of Nantes, France. He earned his Ph.D. degree in Automatic in 1987 and his research degree for leading research and PhD students in 2006. He has been engaged in research for more than 25 years and his research interests include mechanical systems under actuated legged robots, bipedal, nonlinear observers, and biomechanics. He has publications on journals circulated internationally and premier conferences. He is also a topic editor of "International Journal of Advanced Robotic Systems" and member of the editorial board of the journal "Multibody system dynamics".

Maxime Gautier received the Doctorat d'Etat degree in robotics and control engineering from University of Nantes, Nantes, France, in 1990. Since 1991, he has been a Professor of automatic control with University of Nantes. He carries out his research with the Robotics Team, Institut de Recherche en Communications et Cybernétique de Nantes. His research interests include modelling, identification, and control of robots.